Plasma Science and Technology

PAPER

Manipulation and optimization of electron transport by nanopore array targets

Plasma Sci. Technol. **23** (2021) 015001 (7pp) https://doi.org/10.1088/2058-6272/abbd37

Manipulation and optimization of electron transport by nanopore array targets

Yue YANG (杨月)[1], **Boyuan LI** (李博原)[2], **Yuchi WU** (吴玉迟)[1], **Bin ZHU** (朱斌)[1], **Bo ZHANG** (张博)[1], **Zhimeng ZHANG** (张智猛)[1], **Minghai YU** (于明海)[1], **Feng LU** (卢峰)[1], **Kainan ZHOU** (周凯南)[1], **Lianqiang SHAN** (单连强)[1], **Lihua CAO** (曹莉华)[3,4], **Zongqing ZHAO** (赵宗清)[1], **Weimin ZHOU** (周维民)[1] **and Yuqiu GU** (谷渝秋)[1,4]

[1] Laser Fusion Research Center, China Academy of Engineering Physics, Mianyang 621900, People's Republic of China
[2] Key Laboratory for Laser Plasmas (Ministry of Education), School of Physics and Astronomy, Shanghai Jiao Tong University, Shanghai 200240, People's Republic of China
[3] Institute of Applied Physics and Computational Mathematics, Beijing 100088, People's Republic of China
[4] Key Laboratory of HEDP of the Ministry of Education & CAPT, Peking University, Beijing 100871, People's Republic of China

E-mail: liby1990@sjtu.edu.cn and yqgu@caep.cn

Received 15 July 2020, revised 29 September 2020
Accepted for publication 30 September 2020
Published 13 November 2020

Abstract

The transport of sub-picosecond laser-driven fast electrons in nanopore array targets is studied. Attributed to the generation of micro-structured magnetic fields, most fast electron beams are proven to be effectively guided and restricted during the propagation. Different transport patterns of fast electrons in the targets are observed in experiments and reproduced by particle-in-cell simulations, representing two components: initially collimated low-energy electrons in the center and high-energy scattering electrons turning into surrounding annular beams. The critical energy for confined electrons is deduced theoretically. The electron guidance and confinement by the nano-structured targets offer a technological approach to manipulate and optimize the fast electron transport by properly modulating pulse parameters and target design, showing great potential in many applications including ion acceleration, microfocus x-ray sources and inertial confinement fusion.

Keywords: nanopore array, laser-driven electrons, fast electron transport, electron collimation

(Some figures may appear in colour only in the online journal)

1. Introduction

Fast electrons generated by ultra-intense laser interacting with solid targets have wide applications in microfocus x-ray source [1], positron generation [2], ion acceleration [3] and inertial confinement fusion [4]. However, the self-induced Weibel instability [5] and filamentation [6] during the transport process may inevitably be detrimental to beam divergence and directionality, leading to reduced yield and degenerated beam quality. Therefore, guidance and collimation of laser-driven fast electrons are important to further researches and practical applications.

To optimize the interactions of laser pulses and targets, several novel targets with structured surface, such as metal nanobrushes [7–15], carbon nanotubes [16–18], silicon [19–24] and oxide nano/microwires [25] are proposed to improve the quality of laser-driven fast electron beams, proton acceleration and x-ray emission [15, 26, 27]. Many experiments [11–13, 17–19] and relevant simulations [7, 8, 28–31] on femtosecond laser facilities have demonstrated that tailored nano-array structures are helpful to enhance the absorption efficiency of laser energy as well as to guide the propagation of fast electrons. It is believed that the increased absorption depth, surface-to-volume ratio and high local

electric fields of these kinds of targets can contribute to the enhancement of laser absorption, thus greatly enhancing the temperature of hot electrons and hard x-ray generation [7, 11, 15, 32]. On the other hand, the propagation of fast electrons within nano-arrays is affected by both magnetic fields induced by return currents and sheath electric fields on the target surface [9, 33]. Therefore, by using this kind of target, one can artificially construct some aligned micro/nano channels along a certain direction to keep fast electrons propagating inside, and effectively suppress the spread of the beam.

However, the features of nano-structured targets were intensively investigated using ultra-short pulses, while there are only a few studies on the interaction of nano-structures with picosecond laser pulse [9, 12, 16, 34]. Under longer pulse duration, such targets may quickly collapse even with high pulse contrast. Moreover, the ionized plasma density of nano-structures is lower than that of bulk targets, making the subsequent interactions more unstable and uncontrollable. Nevertheless, some preliminary works have already observed enhanced laser absorption and fast electron generation by nano-structured targets irradiated by picosecond lasers [12, 16, 34]. Our simulations showed that fast electrons can be effectively collimated for sub-picosecond interactions, attributed to the confinement of earlier magnetic filaments and later resistive magnetic fields [9]. Therefore, it is necessary to further explore the characteristics and mechanism of the interactions between nano-structured targets and picosecond lasers. Once the advantages of nano-structured targets under longer laser pulse can be proved, the enhanced conversion efficiency and generation of high-charge collimated fast electrons would bring significant contribution to applications including brilliant x-ray sources, proton acceleration and positron generation.

In this work, we study the fast electron transport in tailored nanopore array (NPA) targets irradiated by sub-picosecond pulse lasers. The effective guidance of fast electrons has been confirmed in experiments, and two distinct transport patterns in nano-structured targets are found to result in different characteristics of target-back electron beams. The influence factors and parameter requirement for the electron confinement are obtained by theoretical analysis. As expected, we hope to achieve the guidance and collimation of fast electrons by means of pulse modulation and target design.

This paper is organized as follows. Section 2 introduces the experimental settings and results, which show different electron characteristics after the transport inside NPA targets. Section 3 gives a theoretical model to clarify the underlying mechanism and parameter relation for electron confinement in nano-structured targets. Particle-in-cell (PIC) simulations in section 4 further prove two distinct transport patterns of fast electron bunches in the NPA, and explain the physical phenomena in experiments. Finally, the conclusions are given in section 5.

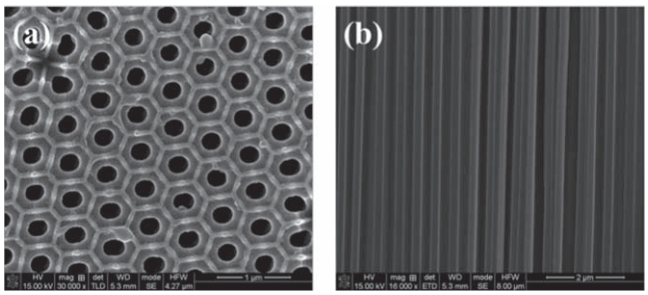

Figure 1. Scans of the anodic aluminum oxide NPA perpendicular to (a) and along the axis (b). Transverse area of the sandwiched NPA is 2 mm × 2 mm.

2. Experiment setup and results

The experiment was carried out using the sub-picosecond laser [0.8 ps (FWHM), 50–150 J, 1.053 μm wavelength, contrast $>5 \times 10^8$] at XingGuang-III laser facility [35]. The pulse was focused by an $f/2.6$ off-axis parabola to a 20 μm (FWHM) focal spot on the target surface. The peak laser intensity could get close to 10^{20} W cm^{-2} with the maximum energy of 150 J. At this laser intensity, fast electrons can be effectively accelerated along the laser propagation direction by the $\boldsymbol{J} \times \boldsymbol{B}$ heating [36] dominantly or along the target normal by the resonant absorption [37]. To clearly identify the beam guiding effect, the laser was set to be s-polarized and incident with an angle of 20° from the target normal. An anodic aluminum oxide template with 250 nm diameter, 550 nm distance and 60 μm thickness NPAs was used as the NPA target (see figures 1(a) and (b)). The arrays are perpendicular to the target surface. Generally, the inherent prepulse or amplified spontaneous emission (ASE) before the main pulse irradiating the target may damage the nano-structures and generate a scale of plasmas blocking the nanopores [38]. To avoid these adverse effects, we have utilized the magnetron sputtering technique to plate a 2 μm Mo layer (front) and a 3 μm Cu layer (back) on the target surface to protect the NPAs. And later, the experimental results will prove that the level of prepulse and preplasmas could not substantially influence the manipulation and optimization of fast electron transport by the NPA targets.

The beam guidance of the NPA was first examined by measuring the propagating direction of fast electrons using image plate (IP, Fuji BAS-SR) stacks. Since the proportion and the energy deposition efficiency of x-rays are much less than that of electrons, the x-ray signals on the IPs can be ignored compared to electron signals. The stack consists of Cu filters and four layers of IPs, as shown in figure 2(a). Electrons with energies above 0.2, 0.5, 1.0 and 1.7 MeV can be detected by the four IPs, respectively. The IP stack was 150 mm away from the target. An angular deviation of 6° was set between the normals of the target and stack. As a result, the signals on the first three IPs are mostly saturated. Figure 2(b) shows the image of the 4th IP, which indicates that most fast electrons propagated along the normal of the NPA (at the direction of +6°) instead of the laser axis where

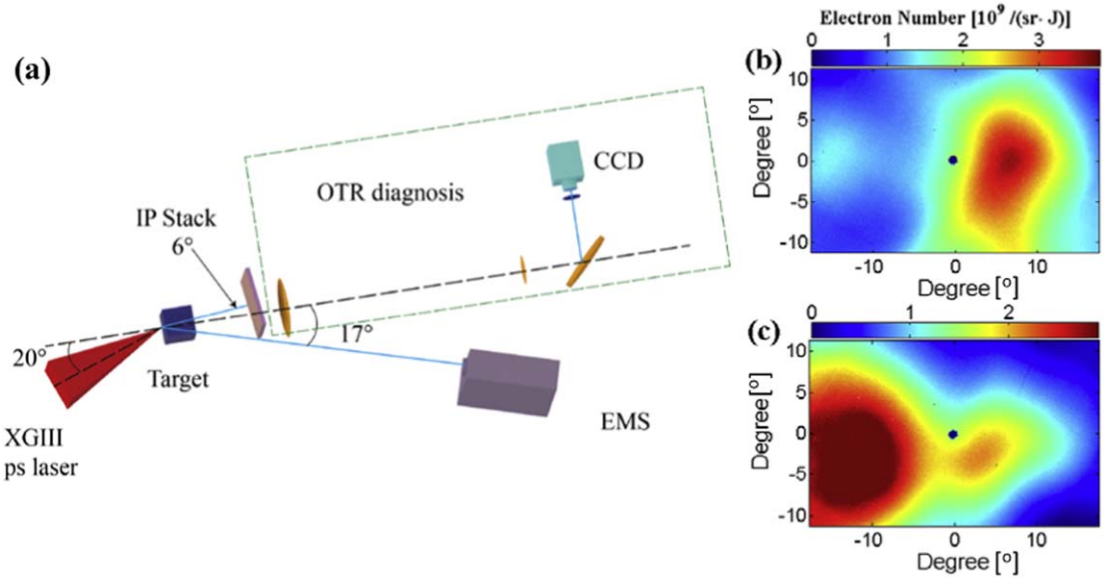

Figure 2. (a) Schematic setup of the experiment. IP stack was 150 mm away from the target. Angular distributions of fast electrons (>1.7 MeV) from the sandwiched NPA (b) and planar target (c).

they were produced by $\boldsymbol{J} \times \boldsymbol{B}$ heating. For comparison, the electron divergence from a 70 μm thick planar Al_2O_3 target is also measured and plotted in figure 2(c). It can be seen that the fast electrons from the planar target mainly transported along the laser axis (at the direction of $-14°$) with a large divergence angle. In contrast, the emission angle of electrons from the NPA target is 14° (FWHM), far less than previous measurements of 30°–40° [39]. Therefore, properly designed NPA targets can not only guide the fast electrons transporting along the nanopore axis, but improve the beam divergence by effective magnetic confinement, even under sub-picosecond pulse lasers.

Then, the optical transition radiation (OTR) measurement was employed to characterize the electron transport in the NPA. It makes use of the characteristic 527 nm light radiated by the fast electrons at the Cu-vacuum interface. To demonstrate the total experimental layout, we put the diagnostic devices of the IP stack and OTR measurement in the same figure, even though the data were measured in separate shots. As shown in figure 2(a), the optical system was normal to the target with a magnification of 7.9. The light was recorded by a 16-bit optical charge coupled device (CCD). A bandpass filter (527 $\pm$ 12 nm) was laid before the CCD to single out the characteristic light, and an electron spectrometer (ESM) was placed at 17° from the target normal to measure the electron spectrum. From the luminance of the OTR, we can get the spatial distribution of fast electron beams at the target back. Figures 3(a) and (b) display the OTR results with laser energies of 140 and 50 J, respectively. The electron spectra of the two cases are shown in figure 3(c). In figure 3(a), a series of equally spaced ring-like signals appear encircling a bright spot, implying that in-target fast electrons transport annularly as multiple bunches surrounding the central collimated beam. The interval between two adjacent rings is roughly 8.2 μm, 15 times the nanopore distance. In figure 3(b), the fringe rings become faint as the laser energy and intensity get lower, corresponding to the decreased number of high-energy electrons and lower effective temperature shown in figure 3(c). On the other hand, a pair of twin spots with a distance around 15–20 μm (less than the laser FWHM) are always found in the center of the rings. This beam pattern implies the strong filamentation of collimated fast electrons, and the branch-off may be due to the repulsion of refluxing electrons in the backside Cu layer.

3. Theoretical analysis

To explain and discuss the experimental results, we analyze the status of fast electron transport in NPA targets. According to previous researches [7, 9], there are basically two self-generated fields in nano-structured targets radiated by ultra-intense laser pulses: the sheath electric fields and toroidal magnetic fields. In nanowire targets, fast electrons will be pushed into the vacuum by the magnetic fields produced by return currents within the nanowires, while the sheath electric fields on the target surface tend to pull the fast electrons back towards the wires. The dynamic equilibrium of electric and magnetic forces keeps fast electrons transporting along the nanowire surface, thus effectively guiding the beam. In this case, fast electrons are hardly affected by direct collisions due to their high kinetic energy ($\nu_{ee,ei} \sim T_e^{-3/2}$). In addition, Li [9] found that sheath electric fields around the nanowires are negligible after a few hundred femtoseconds due to the plasma expansion. Therefore, the magnetic fields play a major role in the transport process of fast electrons.

Similarly, in NPA targets, periodic magnetic fields are generated perpendicular to the propagating direction as return currents transport between nanopores, thus confining the movement of electrons in the vacuum, as shown in figure 4. According to Ampere's law, the average magnetic field

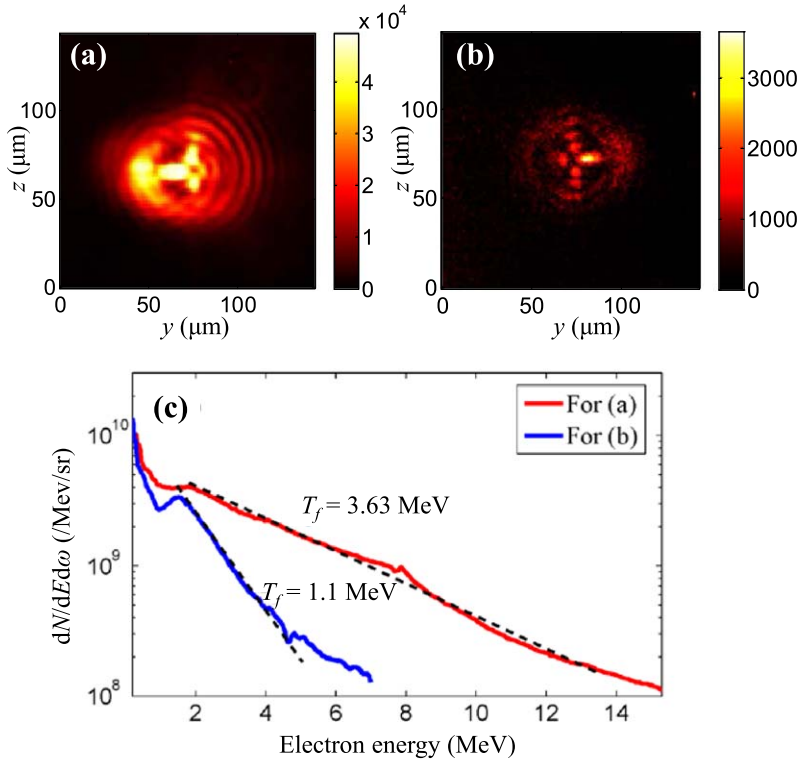

Figure 3. (a), (b) OTR results with different laser energies (shown in (c)). Laser was obliquely pointed to the left. (c) Electron spectra for (a) laser energy of 140 J (red) and (b) laser energy of 50 J (blue). ESM signal was denoised by using the median filter.

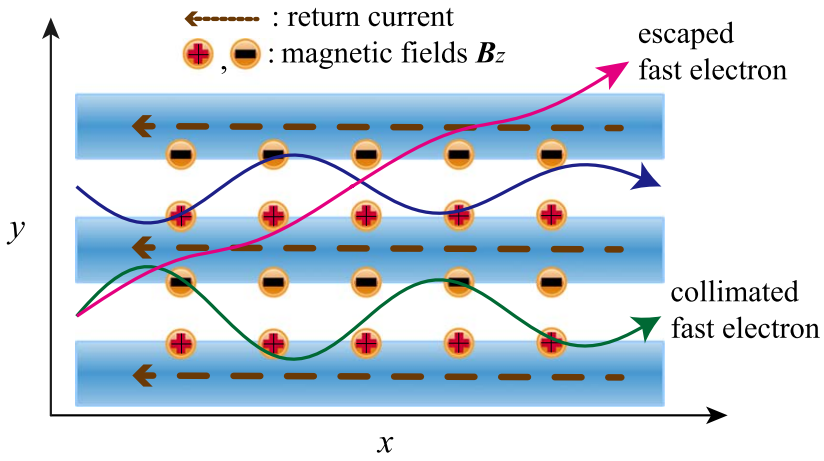

Figure 4. Sketch of fast electron movement and magnetic field generation in the NPA.

around each filament is,

$$\boldsymbol{B}_z = \frac{\mu_0 e n_\mathrm{f} \boldsymbol{v}_\mathrm{f} D_\mathrm{npa}}{4}, \tag{1}$$

where e is the electron charge, n_f is the fast electron density, $\boldsymbol{v}_\mathrm{f}$ is the fast electron velocity and D_npa is the distance between two adjacent nanopores. When a fast electron propagates into the array with a divergence angle θ and Lorentz factor γ, this electron will be confined in a nanopore if its Larmor radius $r_\mathrm{L} = \gamma m_\mathrm{e} \boldsymbol{v}_\mathrm{f} / e\boldsymbol{B}_z$ meets the condition of,

$$r_\mathrm{L} < \frac{D_\mathrm{npa}}{2(1 - \cos\theta)}. \tag{2}$$

Then, substituting the expression $n_\mathrm{f} = I_\mathrm{abs} / \boldsymbol{v}_\mathrm{f} T_\mathrm{f}$ (where I_abs is the absorbed laser intensity and T_f is the fast electron temperature) into equation (2), we can obtain the critical energy for confined fast electrons:

$$E_\mathrm{cr}(\mathrm{eV}) = \frac{\mu_0 c I_\mathrm{abs} D_\mathrm{npa}^2}{8 T_\mathrm{f}(1 - \cos\theta)} - \frac{m_\mathrm{e} c^2}{e}, \tag{3}$$

above which fast electrons cannot be kept within the original nanopore and will escape from the central region. This expression implies that the ability of an NPA target for electron confinement depends on the laser intensity, electron properties and nano-structure spacing. Therefore, fast electrons of different energy ranges will transport with distinct

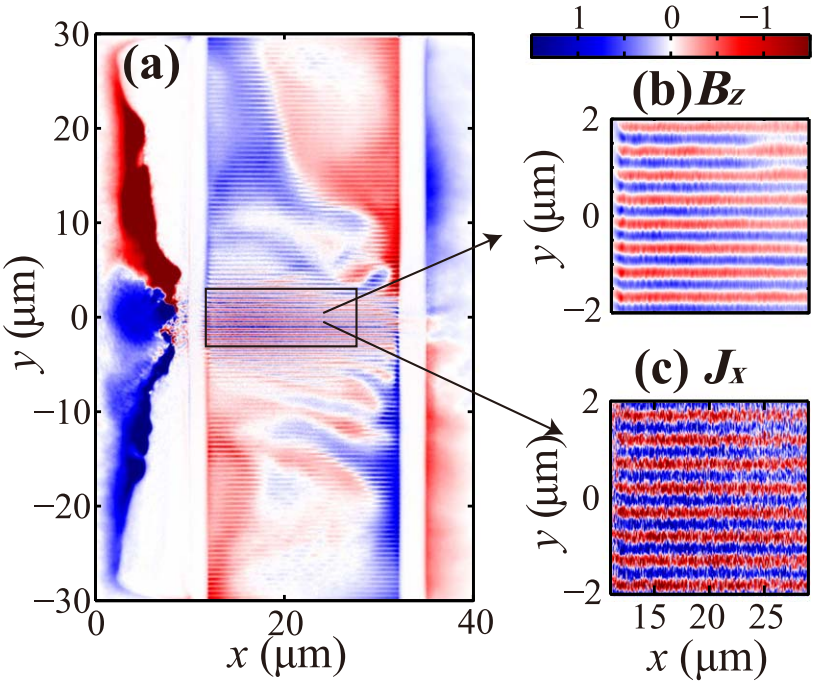

Figure 5. (a) Profile of $\boldsymbol{B}_z$ at $t = 600$ fs, (b) zoom-in of the local magnetic field marked in (a), (c) electron current density $\boldsymbol{J}_x$ in the local region marked in (a). Magnetic field and current density are normalized by $m_e\omega/e$ and $en_c c$, respectively.

patterns, and may result in different spatial distributions at the target back.

4. PIC simulation

Based on the analysis above, we have performed 2D PIC simulations to confirm the physical phenomena of the propagation of fast electrons in NPA targets. We note that the effective temperature and divergence of fast electrons generated by $\boldsymbol{J} \times \boldsymbol{B}$ heating are not related to the laser polarization [40]. Therefore, the transport of the electron beam, which depends on its temperature, divergence and the target configuration can be assumed isotropic, and the 2D simulations can help to understand and interpret mechanisms of acceleration and transport of fast electrons in NPA targets. The code we use is the Opic2D (2D3V) [41], a relativistic kinetic code that includes relativistic binary collisions (e−e, e−i and i−i) and dynamic ionizations (field and impact ionizations). In the simulation, the target configuration is the same as that in experiments, comprising Mo (2 μm) + Al (20 μm, NPA) + Cu (3 μm) with initial ionization degrees of 6, 3 and 2. The NPA consisting of wires and pores of 250 nm width is periodic in the transverse direction. Limited by the computation capacity, the ion density of each layer is $12n_c$ for Mo, $11n_c$ for Al and $15n_c$ for Cu, where n_c is the critical plasma density. Considering the preplasmas produced on the target surface, and combining actual laser parameters [35], we put molybdenum preplasmas whose density exponentially decreases from 10 to $0.06n_c$ with a scale length of 2 μm in front of the target.

The s-polarized laser at $\lambda = 1$ μm wavelength is obliquely incident with an angle of 20° from the target normal. The pulse has an envelope profile of $a = a_0 \exp(-r^2/\sigma^2)\sin(\pi t/\tau)$, where $a_0 = 8.5$ is the peak amplitude of the laser field, $\sigma = 4.2$ μm is the laser radius and $\tau = 800$ fs is the laser duration. Fourth-order interpolation is used to relax the restriction on the grid size by Debye length. Each cell contains macro-particles of 16 electrons and four ions. Absorptive boundary conditions are used for both fields and particles.

We first investigate the electron transport and magnetic confining effects at an earlier time. Figure 5(a) shows the azimuthal magnetic field $\boldsymbol{B}_z$ at $t = 600$ fs. As expected, the magnetic fields close to the Mo substrate are periodic in the y direction and tend to push fast electrons into the vacuum. Locally, as shown in figures 5(b) and (c), fast electron beams in the central region are brushed into filaments and just encircle the magnetic fields, indicating the constraint of the magnetic fields. However, some electrons are too energetic to be properly restricted, and they may scatter across the nanopores, resulting in macro channels in the fringe region shown in figure 5(a). Moreover, the distribution of fast electrons near the target back becomes disordered due to the beam filamentation and repulsion of refluxing electrons.

To validate our analysis above, we further explore the transport patterns of fast electrons in the NPA in terms of their energy range. According to our prediction, fast electrons propagating inside the target can be divided into two components: the central confined low-energy electrons and the escaped high-energy electrons. From the electron spectrum, the temperature of fast electrons is $T_f = 3.86$ MeV with a profile of $f(E) = \exp(-E/T_f)/T_f$, roughly consistent with Wilks' ponderomotive scaling law [36]. The electron divergence angle of 35° and the absorption efficiency of 30% are also obtained in the simulation. Therefore, the critical confined energy calculated from equation (3) is $E_{cr} \approx 5$ MeV.

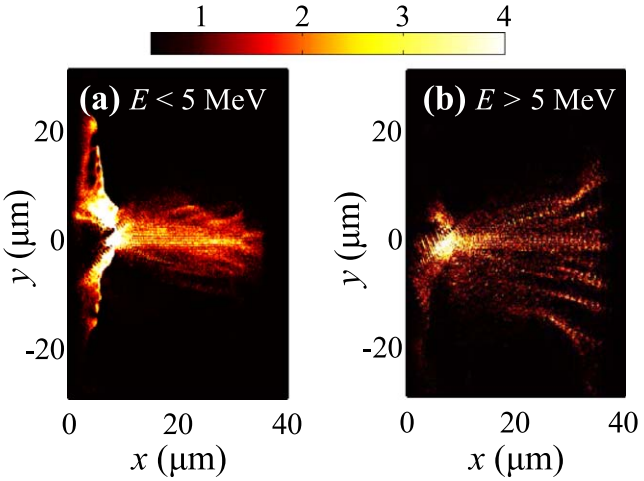

Figure 6. Spatial distributions of energy density of electrons with (a) $E < 5$ MeV and (b) $E > 5$ MeV at $t = 600$ fs. Energy density is normalized by $n_c m_e c^2$.

Based on the critical energy, the spatial distributions of energy density of the two kinds of fast electrons are shown in figure 6. We can find that the low-energy electrons with $E < 5$ MeV are excellently guided and collimated in the central region, with the beam filamentation in size of the nanopore diameter, far smaller than the focal spot.

On the other hand, high-energy electrons scatter around and form couples of bunches with approximately the same intervals (see figure 6(b)). The bunch spacing gets greater as the transport distance increases, and it becomes 3.5–4 μm at the target back, about 7–8 times the nanopore distance and in accordance with the distribution of magnetic fields in figure 5(a). The underlying physics of the macro self-channeling of energetic electrons can be explained by the accumulated confining effect of magnetic fields. Although the electrons above E_{cr} cannot be restricted in one nanopore, they will be re-pinched under the suppression of multiple periodic magnetic fields after traveling across multi-nanopores, thus emerging into bunches with similar intervals. Once macro magnetic channels are generated under the magnetic confining effect, the beam pinch will be further enhanced by the resistive annulus effect [42].

Compared to experimental results, the simulations reproduce similar forms of electron distributions at the backside of the targets, verifying our theoretical deductions. We note that the different bunch spacings may due to the differences in simulation parameters and dimensions. The faint signal of fast electrons at the fringe region for lower-energy laser (see figures 3(a) and (b)) can be explained, since the energetic electrons (above the critical confined energy), which would transport as annular bunches on the periphery profoundly reduced (see figure 3(c)). These results prove the two distinct transport patterns of fast electrons and the appearance of macro magnetic channels, validating the important role of self-generated periodic magnetic fields. To conclude, fast electrons transporting in the NPA would turn into two components: central confined low-energy beam and fringe annular high-energy bunches. According to our analysis, the critical energy of confined electrons in NPAs could be altered by changing the laser intensity and nanopore distance. Therefore, we can possibly select and obtain fast electrons in terms of their energy and divergence with proper parameter modulation. The transport of fast electrons can be artificially manipulated to provide electron beams with specific characteristics, offering facilities for subsequent practical applications and researches.

5. Conclusion

In summary, an NPA target is proposed to guide and collimate fast electrons driven by picosecond pulse lasers. Experimental results proved the effective electron guidance of NPA targets under sub-picosecond-pulse lasers. Different transport patterns of fast electrons are found as we observed the collimated central beams and surrounding ring-like electron bunches at the target back. By theoretical analysis and derivation, we obtained the critical energy for confined fast electrons in NPA, which depends on the laser intensity, electron properties and nano-structure spacing. PIC simulations further confirmed the physical phenomena and intrinsic schemes of electron transport dominated by periodic magnetic fields. It is found that low-energy electrons can be initially restricted in the center, while high-energy scattered electrons would be re-pinched into macro channels by the accumulated magnetic confining effects, in good accordance with the experiments.

This finding provides a way to manipulate the electron transport and spatial distribution by pulse modulation and target design, thus selecting and optimizing fast electrons with specific characteristics, which has great potential in practical applications including microfocus x-ray sources, positron generation, ion acceleration and inertial confinement fusion.

Acknowledgments

This work was supported by the National Key R&D Program of China (Grant No. 2016YFA0401100), the Science and Technology on Plasma Physics Laboratory (Grant Nos. 6142A04180201 and JCKYS2020212006), National Natural Science Foundation of China (Grant No. 11975214) and the Science Challenge Program (Grant Nos. TZ2016005 and TZ2018005).

References

[1] Park H S *et al* 2006 *Phys. Plasmas* **13** 056309
[2] Chen H *et al* 2015 *Phys. Rev. Lett.* **114** 215001
[3] Zhuo H B *et al* 2013 *Phys. Plasmas* **20** 093103
[4] Robinson A P L *et al* 2014 *Nucl. Fusion* **54** 054003
[5] Weibel E S 1959 *Phys. Rev. Lett.* **2** 83
[6] Sentoku Y *et al* 2002 *Phys. Rev. E* **65** 046408
[7] Cao L H *et al* 2010 *Phys. Plasmas* **17** 043103
[8] Andreev A A, Nickles P V and Platonov K Y 2014 *Plasma Phys. Control. Fusion* **56** 084005
[9] Li B Y *et al* 2015 *Phys. Plasmas* **22** 123118

[10] Wang J *et al* 2015 *Chin. Opt. Lett.* **13** 031001
[11] Zhao Z Q *et al* 2010 *Phys. Plasmas* **17** 123108
[12] Khaghani D *et al* 2017 *Sci. Rep.* **7** 11366
[13] Lübcke A *et al* 2017 *Sci. Rep.* **7** 44030
[14] Hollinger R *et al* 2017 *Optica* **4** 1344
[15] Mondal S *et al* 2011 *Phys. Rev.* B **83** 035408
[16] Habara H *et al* 2016 *Phys. Plasmas* **23** 063105
[17] Ji Y L *et al* 2010 *Appl. Phys. Lett.* **96** 041504
[18] Chatterjee G *et al* 2012 *Phys. Rev. Lett.* **108** 235005
[19] Singh P K *et al* 2012 *Appl. Phys. Lett.* **100** 244104
[20] Cristoforetti G *et al* 2014 *Plasma Phys. Control. Fusion* **56** 095001
[21] Cristoforetti G *et al* 2017 *Sci. Rep.* **7** 1479
[22] Jiang S *et al* 2014 *Phys. Rev.* E **89** 013106
[23] Jiang S *et al* 2016 *Phys. Rev. Lett.* **116** 085002
[24] Black D S *et al* 2019 *Phys. Rev. Lett.* **122** 104801
[25] Samsonova Z *et al* 2017 *AIP Conf. Proc.* **1811** 180001
[26] Andreev A A *et al* 2019 *Phys. Plasmas* **26** 113110
[27] Lécz Z and Andreev A 2017 *Phys. Plasmas* **24** 033113
[28] Cao L H *et al* 2011 *Phys. Plasmas* **18** 054501
[29] Wang H *et al* 2012 *Laser Part. Beams* **30** 553
[30] Yu J Q *et al* 2012 *Appl. Phys. Lett.* **100** 204101
[31] Fedeli L *et al* 2018 *Sci. Rep.* **8** 3834
[32] Kulcsár G *et al* 2000 *Phys. Rev. Lett.* **84** 5149
[33] Wang J *et al* 2014 *Phys. Plasmas* **21** 103111
[34] Sedov M V *et al* 2019 *Laser Part. Beams* **37** 176
[35] Zhu Q H *et al* 2018 *Laser Phys. Lett.* **15** 015301
[36] Wilks S C *et al* 1992 *Phys. Rev. Lett.* **69** 1383
[37] Freidberg J P *et al* 1972 *Phys. Rev. Lett.* **28** 795
[38] Gibbon P and Rosmej O N 2007 *Plasma Phys. Control. Fusion* **49** 1873
[39] Green J S *et al* 2008 *Phys. Rev. Lett.* **100** 015003
[40] Li B Y *et al* 2016 *Phys. Plasmas* **23** 093121
[41] Zhang Z M *et al* 2012 *Appl. Phys. Lett.* **100** 134103
[42] MacLellan D A *et al* 2013 *Phys. Rev. Lett.* **111** 095001